Modified thick thermal barrier coatings: Thermophysical characterization

S. Ahmaniemi[a,*], P. Vuoristo[a], T. Mäntylä[a], F. Cernuschi[b], L. Lorenzoni[b]

[a]*Tampere University of Technology, Institute of Materials Science, PO Box 589, 33101 Tampere, Finland*
[b]*Cesi, Via Reggio Emilia, 39, 20090 Segrate, Italy*

Abstract

Thermophysical properties of modified zirconia based thick thermal barrier coatings ($8Y_2O_3$–ZrO_2, $25CeO_2$–$2.5Y_2O_3$–ZrO_2 and $22MgO$–ZrO_2) were characterized at temperature range of RT-1300 °C. Coatings were studied in laser-glazed and phosphate sealed state, and their properties were compared to as-sprayed coatings. Laser glazing affected only slightly on thermal conductivity of the studied coatings. If the segmentation cracks, induced by laser glazing, were oriented vertically like in the case of laser-glazed $8Y_2O_3$–ZrO_2 coating, thermal conductivity was increased in some degree. But if the orientation of the segmentation cracks was deviated from the vertical direction or if the cracks were branched, thermal conductivity was decreased. This was the case with the laser-glazed $25CeO_2$–$2.5Y_2O_3$–ZrO_2 and $22MgO$–ZrO_2 coatings. Phosphate based sealing treatments were found to increase the thermal conductivity of all coatings. Aluminium phosphate sealing also lowered the high temperature stability of the $8Y_2O_3$–ZrO_2 coating down to 1000 °C. In $8Y_2O_3$–ZrO_2 and $25CeO_2$–$2.5Y_2O_3$–ZrO_2 based coatings thermal conductivity was increased in consecutive measurement cycles, caused mainly by the sintering based phenomena in which the contact between overlapping lamellae was improved. Thermal conductivity of the $22MgO$–ZrO_2 based coatings was increased significantly in the first measurement cycle because of the unstabilization of zirconia-caused by precipitation of MgO.
© 2003 Elsevier Ltd. All rights reserved.

Keywords: Coatings; Functional applications; TBC; Thermal barrier coatings; Thermal properties; ZrO_2

1. Introduction

Better thermal insulation of the hot path components is needed in state-of-the-art gas turbines and diesel engines because of the increasing demands of the higher process temperatures. In these processes, the component surface temperatures are mainly controlled by thermal barrier coatings (TBCs) and various cooling techniques. For that reason low thermal conductance (thermal conductivity of the coating/coating thickness) TBCs are extensively studied. Lowering of thermal conductance of TBCs can be approached three ways: (1) lowering the thermal conductivity of the coating material, (2) lowering the thermal conductivity by increasing the porosity of the coating and (3) increasing the thickness of the coating. When tailoring the low thermal conductance

TBCs, all these ways should be considered. Klemens et al. [1–3] have lately published comprehensive studies of the theory of thermal conductivity of zirconia based TBCs. In those papers the heat conduction of TBCs was considered to occur by two separate mechanisms, namely lattice waves and radiation. As a basis of these mechanisms the heat conduction–microstructure relation of TBCs was discussed. Nicholls et al. [3] used terms phonon and photon conductivity when referring to the same lattice vibration (waves) and radiation mechanisms. Nicholls has presented promising results of lowering thermal conductivity of TBCs by reducing phonon and photon transport. This was obtained by introducing one or two dimensional defects into the zirconia structure by dopants or by layered microstructures. There has been also other studies focused on lowering thermal conductivity of TBCs.[4–7] In general there is lots of published data available of determining thermal properties plasma sprayed TBCs. Some of the studies[8–10] handles thermal properties only in the as-sprayed state, but

---

some[11–17] take into consideration also the effect of thermal ageing. The effect of porostity on thermal conductivity is also discussed in some context.[18] Nowadays almost all the thermal diffusivity measurements of TBCs are performed with the laser flash equipment for free standing coatings and it seems to be rather accurate method if the input parameters and test setup are correct.[19,20] Even the laser flash method seems to be most used method, there are still other methods in use.[19,21,22] In addition to practical laboratory measurements lots of effort has been put on modelling the thermal properties of TBCs as a function of different microstructures.[21,23,24]

In the first part of this study (*Modified Thick Thermal Barrier Coatings, Part I: Microstructural Characterization*)[25] these TTBCs were extensively characterised. We showed that with the coating modification processes, such laser-glazing and phosphate based sealing, the surface of these TTBCs can be densified. Surface densification is one method in improving the hot corrosion resistance of TTBCs, but also enhancing their erosion resistance. It is also expected that the vertical segmentation cracks, induced by laser-glazing, could increase the strain tolerance of the thick coatings. In addition to $8Y_2O_3$–ZrO_2, $25CeO_2$–$2.5Y_2O_3$–ZrO_2 and $22MgO$–ZrO_2 coatings were selected to this study for seeking better hot corrosion resistant materials for diesel engine process.

In this paper it was characterized the thermophysical properties of the modified zirconia based thick thermal barrier coatings (TTBCs). Thermal diffusivity $\alpha(T)$, specific heat $C_P(T)$ and bulk density ρ_B was determined in order to obtain data for coating thermal conductivity calculations [$k(T) = \alpha(T)*C_P(T)*\rho_B$]. Results of thermal expansion and microstructural characterization studies are also presented for better understanding of the thermal property–microstructure relationship.

2. Experimental

2.1. Materials

Three different TTBCs ($8Y_2O_3$–ZrO_2, $25CeO_2$–$2.5Y_2O_3$–ZrO_2 and $22MgO$–ZrO_2) were sprayed with air plasma spray (APS) system (Plasma-Technik A3000S, Sulzer Metco AG, Wohlen, Switzerland). Coating thicknesses were at the range of 700–1000 μm and coatings were sprayed on AISI4142 steel substrates. Freestanding coatings were prepared by removing them from the substrates by chemical etching using 50/50 HCl/H_2O solution. For thermal diffusivity and specific heat measurements disk shaped specimens ($\varnothing = 10$ mm and $\varnothing = 6$ mm respectively) were prepared from the freestanding coating disks ($\varnothing = 25$ mm). For all other purposes the specimens were prepared from the flat-shaped (10×60 mm) freestanding coatings.

In addition to the as-sprayed coatings we studied some modified TTBC structures. Coating microstructures were modified by laser-glazing and phosphate based sealing treatments. In laser-glazing process the coating surface (50–150 μm) was melted by continuous wave Nd-YAG laser beam. Laser-glazing was performed before the coating removal from the substrates. In phosphate based sealing treatments the sealant was impregnated into the coatings and heat treated at 300 °C for 4 h. $8Y_2O_3$–ZrO_2 and $25CeO_2$–$2.5Y_2O_3$–ZrO_2 coatings were sealed by aluminium phosphate based sealant and $22MgO$–ZrO_2 coating by orthophosphoric acid. Phosphate based sealing treatments were carried out for free-standing specimens in order to avoid possible sealant reactions with the etchant. More detailed description of manufacturing the modified TTBC as well as of their microstructural characterization can be found from refs.[25–27] In Table 1 there is presented abbreviations for all coating compositions.

Some coatings were heat treated at 1250 °C in air for 5 h for the purpose of microstructural characterization. Abbreviation for the heat treatment is HT. The heat treated specimens were aimed to simulate the microstructural conditions of the thermal diffusivity specimens.

2.2. Microstructural characterization

Coating microstructures were studied with optical microscope (Leitz, Wetzlar, Germany) and scanning electron microscope (ESEM, Model XL-30, Philips, Eindhoven, Netherlands). The phase structures were characterized by image plate X-ray diffractometer (XRD, Italstructures, Riva del Garda, Italy) using filtered CuK_α radiation operated at 40kV and 30mA. The used exposure time was two hours and the XRD spectra were analyzed in 2θ-range of 20–120°. XRD analysis for the phosphate sealed coatings were made after grinding approximately 50 μm layer from the surface, because reaction products on the coating surface normally differ

Table 1
Abbreviations of the coatings

Coating composition	Abbreviation
$8Y_2O_3$–ZrO_2	8Y
$8Y_2O_3$–ZrO_2 (laser-glazed)	8YL
$8Y_2O_3$–ZrO_2 (aluminum phosphate sealed)	8YAP
$25CeO_2$–$2.5Y_2O_3$–ZrO_2	25C
$25CeO_2$–$2.5Y_2O_3$–ZrO_2 (laser-glazed)	25CL
$25CeO_2$–$2.5Y_2O_3$–ZrO_2 (aluminum phosphate sealed)	25CAP
$22MgO$–ZrO_2	22M
$22MgO$–ZrO_2 (laser-glazed)	22ML
$22MgO$–ZrO_2 (orthophosphoric acid sealed)	22MOPA

Table 2
Total and open porosity and bulk density of the coatings before and after the heat treatment

Coating	Total porosity, IA [Vol.-%]		Open porosity, MP [Vol.-%, ±1%]		Open porosity, Archimedes [Vol.-%, ±1%]		Bulk density, Archimedes [g/cm^3, ±0.1 g/cm^3]	
	As-sprayed	Heat treated	As-sprayed	Heat treated	As-sprayed	Heat treated	As-sprayed	Heat treated
8Y	20.7±1.8	9.4±0.6	9.3	10.0	9.0	9.1	5.3	5.4
8YL	2.8±2.6[a]	2.2±0.9[a]	a	a	a	a	a	a
8YAP	12.6±1.9	6.9±1.1	5.3	9.0	3.9	5.9	5.4	5.4
25C	18.4±3.3	9.8±0.6	10.4	8.5	7.5	8.0	5.6	5.7
25CL	4.9±2.1[a]	1.4±0.7[a]	a	a	a	a	a	a
25CAP	12.9±2.4	5.4±0.6	5.4	5.4	5.2	5.4	5.7	5.7
22M	12.1±2.2	8.2±1.1	9.5	13.7	13.4	11.9	4.2	4.5
22ML	3.3±1.6[a]	3.4±1.3[a]	a	a	a	a	a	a
22MOPA	7.5±1.6	12.0±2.0	7.2	9.0	3.9	5.3	4.4	4.8

[a] Reliable porosity measurement for the laser-glazed coatings was possible to perform only by the image analysis. The analyses were taken from the melted top layer.

considerably from those below the surface. Structural quantitative XRD phase analyses were made by the Rietveld method[28,29] using MAUD software (Material Analysis Using Diffraction, version 1.87, Luca Lutterotti, University of Trento, Italy). Total porosity was evaluated by image analysis using optical microscope (Carl Zeiss Axiophot, Germany) and image acquisition and analysis software (QWin, Leica Microsystems, Switzerland). The results and their deviations are presented as a mean value of five separate analyses. Open porosity was measured with mercury porosimetry (models Pascal 140 and Porosimeter 2000, CE-instruments, Milan, Italy) at pressure range 0.1 kPa–200 MPa. Bulk density of the coatings was determined by the method of Archimedes.

2.3. Thermal expansion

Thermal expansion studies were carried out by dilatometer (Adamel Lhomargy, model DI-24, France) in air at temperature range of 50–1300 °C. The temperature ramping rate varied from 5 °C/min to 10 °C/min and dwell times at maximum temperature from 5 min to 5 h. Measurements were performed for both, as-sprayed and heat treated coatings.

2.4. Thermal diffusivity α(T)

Thermal diffusivity $\alpha(T)$ measurements were carried out with laser flash apparatus Theta (Theta Industries Inc., Port Washington, NY, USA) in vacuum (<0.01 Pa). Measurements were performed at seven different temperatures in the temperature range of 100–1300 °C. Measurements were repeated five times at each temperature for statistical reasons. Prior to evaluating the thermal diffusivity, in order to make the sample surfaces opaque, thin layers of colloidal graphite were painted on both the front and the rear faces. Measurement cycle

was repeated three times for each coating in order to find out the effect of high temperature exposure of the previous measurement on $\alpha(T)$.

2.5. Specific heat $C_P(T)$

Specific heat measurements were performed by Differential Scanning Calorimeter DSC 404 C (Netzsch-Gerätebau GmbH, Selb, Germany). The scanning rate was 15 °C/min at the temperature range of 100 up to 1250 °C. Measurements were carried out in air and in argon atmospheres using either alumina or platinum crucibles. Weight of the free-standing coating specimen was approximately 80 mg. For each sample three consequent measurements cycles were performed in order to lower statistical error of the measurement.

2.6. Thermal conductivity k(T)

Thermal conductivities $k(T)$ were calculated using the equation $k(T) = \alpha(T) * C_P(T) * \rho_B$, where ρ_B is the bulk density of the coating. Thermal conductivity values were calculated in 50 °C intervals at temperature range of 150–1250 °C. For these temperature points the thermal diffusivity data was interpolated from the original data.

3. Results and discussion

3.1. Microstructural characterization

Coatings were characterized by their microstructure and phase structure before and after the heat treatment in order to better explain the effect of irreversible structural changes that occurred during the high temperature measurement cycles. Table 2 gives the coating total and open porosities and bulk densities determined by

Table 3
Quantitative XRD phase analysis results for as-sprayed and heat treated coatings

Coating	m–ZrO_2 [vol-%,±3%]		t'–ZrO_2 [vol-%,±3%]		c–ZrO_2 [vol-%,±3%]		Other phases [vol-%,±3%]	
	As-sprayed	Heat treated	As-sprayed	Heat treated	As-sprayed	Heat treated	As-sprayed	Heat treated
8Y	3	3	92	92	5	5	–	–
8YL	–	–	100	100	–	–	–	–
8YAP	3	50	92	48	5	2	–	Traces of $AlPO_4$[a]
25C	–	–	72	89	25	9	$CeO_2 = 3$	$CeO_2 = 2$
25CL	–	–	96	99	–	–	$CeO_2 = 4$	$CeO_2 = 1$
25CAP	–	5	60	54	39	38	$CeO_2 = 1$, traces of ZrP_2O_7[a]	$CeO_2 = 3$
22M	–	65	19	8	55	1	$MgO = 26$	$MgO = 26$
22ML	–	54	–	–	16	–	$Mg_2Zr_5O_{12} = 66$, $MgO = 18$	$Mg_2Zr_5O_{12} = 29$, $MgO = 17$
22MOPA	–	85	19	3	55	–	$MgO = 26$, traces of ZrP_2O_7[a]	$MgO = 12$

[a] ZrP_2O_7 and $AlPO_4$ were found only at the coating surface. These phases were not detected if the surface layer of 50 μm was grinded off before the XRD analysis
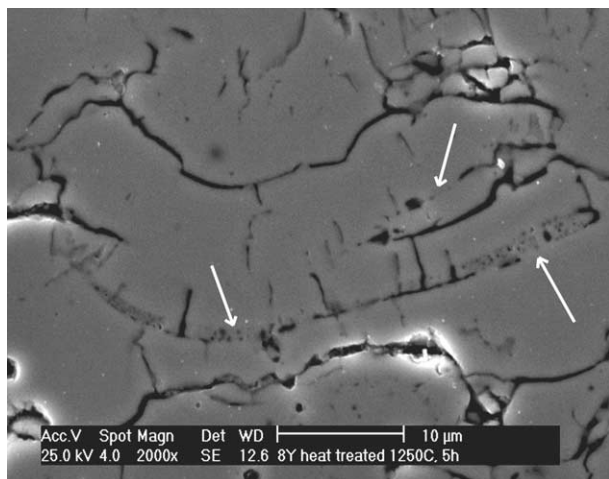

Fig. 1. SEM micrograph of the heat treated 8Y coating. The white arrows point out the improved contact of the lamellae at splat boundaries.

image analysis, mercury porosimetry and method of Archimedes.

The image analysis porosity results did not correspond to the reality due to the pull-outs, found in the coating cross sectional surfaces. Pull-outs are normally identified as pores in image analysis, but they are defects caused by the specimen preparation procedure. However, in the polished cross sectional surfaces of the heat treated coatings the amount pull-outs was significantly decreased. In practice the heat treatment increased the cohesion of the lamellae so for that reason they were not so susceptible to be pulled out. The integrity of the lamellar structure was probably increased due to the sintering based phenomena at splat boundaries. In SEM studies of the heat treated 8Y coating some evidence of the better contact of lamellae were found, see Fig. 1. The

white arrows point out the closed cracks and splat boundaries and remaining string of fine pores.

The open porosities, determined by mercury porosimetry and method of Archimedes, are similar before and after the heat treatment. Sintering based phenomena did not affect seemingly on the open porosity, and no clear evidence of the reduction of the very fine pores was seen in mercury porosimetry. Interpretation of the results of the 22M based coatings was more difficult, because the coating phase structure was not stable in the heat treatment at maximum temperature of 1250 °C. In heat treated coatings the MgO precipitates were seen as dark spots in optical micrographs, which complicated the porosity determination by image analysis. The porosity reduction caused by the phosphate sealing could be seen with all coatings and with all three methods. However, the heat treatment increased the open porosity of the phosphate sealed coatings in some degree. This was probably due to the shrinkage of the sealant at high temperatures, caused by the crystallization of the amorphous sealant. Quantitative XRD phase analysis results for as-sprayed and heat treated coatings are presented in Table 3.

The t–ZrO_2 phase structure of the as-sprayed 8Y and laser-glazed 8YL coatings did not change in the heat treatment. Instead of that in aluminium phosphate sealed 8YAP coating the tetragonal structure was partially unstabilized and 50 vol% of m–ZrO_2 was detected by XRD after the heat treatment. In phosphate sealed coating no crystalline sealant phases were identified by XRD and in TEM studies some amorphous phosphates were seen in the coating microcracks. After the heat treatment traces of $AlPO_4$ were identified in the coating surface and it was assumed also that the amorphous structure of the sealant in the coating cracks was crystallized. However, the amount of the sealant, penetrated
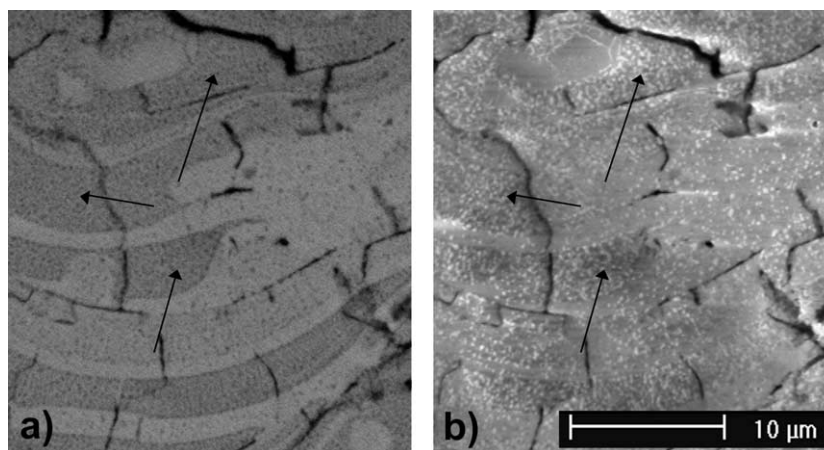
Fig. 2. MgO precipitates in SEM micrographs of the 22M coating, (a) BSE image of the heat treated 22M coating and (b) SE image of the same cross sectional area.

into the coating structure was probably too low for detecting it by XRD. Heat treatment had only slight effect on the microstructure of the ceria stabilized 25C and 25CL coatings. However, 5 vol% of m–ZrO_2 was found in the heat treated 25CAP coating. Magnesia stabilized coatings were strongly affected by the heat treatment. The c– ZrO_2 and t′– ZrO_2 structures were almost totally unstabilized and the major part of the coatings was transformed to m–ZrO_2. Unstabilization of the structure could be detected in SEM studies as precipitation of MgO. The distribution of the precipitates was rather fine and uniform, but in some lamella their number was higher, see the arrows in Fig. 2. In secondary electron image, Fig. 2a, the precipitates can be seen as dark spots and in backscatter electron image, Fig. 2b, as white spots.

3.2. Thermal expansion

In as-sprayed 8Y coating the thermal expansion was linear up to 1000 °C, see Fig. 3a. Coefficient of thermal expansion (CTE) for the as-sprayed coating at temperature range of 50–1000 °C was approximately 9.9×10^{-6} K^{-1}. The 8Y coating showed some shrinkage in the temperatures of 1000–1300 °C, but not any phase changes. In Fig. 3a it can be seen the effect of time on shrinkage. The major shrinkage occurs very fast and there is only slight difference in total shrinkage if the dwell time at the maximum temperature was extended from 5 min to 5 h. In the heat treated coating the total shrinkage [dl/l_o] of the measurement cycle was very limited and it was only ∼10% of the shrinkage of the as-sprayed coating (0.023% vs. 0.275%). In aluminium phosphate sealed 8YAP coating the thermal expansion behaviour was not so linear in the whole temperature range, see Fig. 3b. If the specimen was heated only up to 980 °C there was no indication of shrinkage or phase changes. But if heated up to 1300 °C some irreversible

behaviour could be observed. For some reason the t′–ZrO_2 phase structure was partially unstabilized at high temperature, which could be seen as a phase changes in the return curve and even more clearly in the case of the heat treated 8YAP coating. This phase change was also detected in XRD studies, presented in previous chapter. The phase change regions (t–ZrO_2 ⇒ m–ZrO_2, m–ZrO_2 ⇒ t–ZrO_2) are marked on the curves with the textured areas in Fig. 3.

In 25C based coatings the thermal expansion behaviour of the as-sprayed and aluminium phosphate sealed coatings was almost equal, see Fig. 3c and d. In both coatings the shrinkage could be seen at the temperature range of 1000–1300 °C without any phase changes. In the heat treated coatings no phase changes were observed, but some minor shrinkage was still possible to detect. CTE for all ceria stabilized zirconia coatings in temperature range of 50–1000 °C was approximately 10.8×10^{-6} K^{-1}.

As-sprayed and sealed magnesia stabilized coatings, 22M and 22MOPA, started to unstabilize at the temperatures of 900–950 °C, see Fig. 3e and f. This could be seen as a strong shrinkage in the both coatings (shrinkage was about 2.566%, so it was even 10 times higher than in 8Y or 25C coatings). As presented in previous chapter the phase structure of both coatings was almost totally changed to m–ZrO_2 in the heat treatment. After the heat treatment the shrinkage of 22M HT and 22MOPA HT coatings was very limited. The phase changes (m–ZrO_2 ⇒ t–ZrO_2 and t–ZrO_2 ⇒ m–ZrO_2) of zirconia could be detected, see the textured areas in the Fig. 3e and f. For some reason the phase changes occurred at higher temperature in the sealed coating 22MOPA HT. CTE of the as-sprayed 22M coating at temperature region of 50–700 °C was approximately 8.8×10^{-6} K^{-1}.

The thermal expansion behaviour of the studied TTBCs indicated both irreversible and reversible
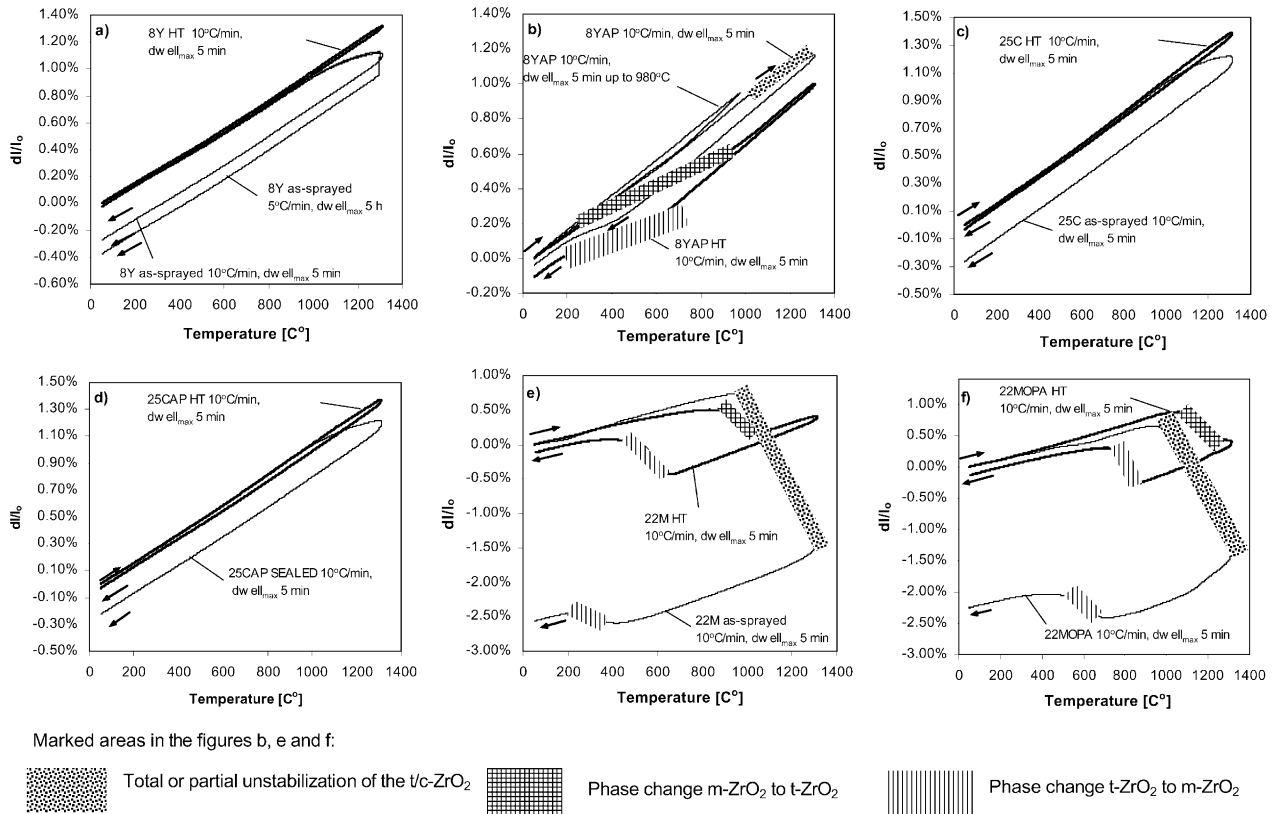
Fig. 3. Thermal expansion of (a) 8Y coatings, (b) 8YAP coatings, (c) 25C coatings, (d) 25CAP coatings, (e) 22M coatings and (f) 22MOPA coatings. Marked areas in the figs. refer to the structural changes of zirconia. Marking textures are explained below the figure.

microstructural changes. The first type of irreversible change was observed in the first measurement cycles of the 8Y and 25C based coatings at temperature range of 1000–1300 °C. This irreversible shrinkage could be caused by sintering based phenomena. Zhu and Miller In ref. [13] presented comparable results of sintering shrinkage of various plasma sprayed TBCs. The second type of irreversible change was seen as strong shrinkage in the case of magnesia stabilized coating when the MgO was precipitated from the zirconia matrix. Reversible microstructural changes were detected as phase changes in totally or partially unstabilized coatings, eg. in heat treated 8YAP, 22M and 22MOPA coatings.

3.3. Thermal diffusivity $\alpha(T)$

Thermal diffusivity of the 8Y coatings was rather temperature independent and agreed well with the literature data,[10,19] see Fig. 4a. The small divergence in the results can be based on different microstructural features of the specimens. Results can be affected also by the scanning rate of temperature used in thermal diffusivity measurement. This means that with slower scanning rates there is more time for irreversible structural changes such as sintering. The accuracy of our measurements was believed to be within 5%. When compared the thermal diffusivity of 8Y based coatings and

their three consecutive measurements of each specimen, Fig. 4b, it can be seen that the thermal diffusivity was higher in the second measurement run for all type coatings. This indicated that some structural changes had taken place during the first run. Instead of that the difference of the second and third runs was rather small. This shows that the microstructural changes had occurred quite rapidly in the first run. The major structural change was obviously the sintering induced better thermal contact of the lamellae, but there could also be some minor irreversible structural changes at crystal lattice scale that have some effect on increase of thermal diffusivity. The plasma sprayed zirconia is normally mixture of m–ZrO_2, t'–ZrO_2 and c–ZrO_2. The lattice parameters of the t'–ZrO_2 and c–ZrO_2 phases might vary locally as the concentration of the stabilizing oxide varies. The plasma sprayed zirconia is also slightly unstoichiometric after spraying, so the structure is quite complex. The first heating cycle up to 1300 °C can change the situation by decreasing the amount of local defects and by restoring the structure to more stable state. However, the measurements were made in vacuum so for example the diffusion of oxygen into the unstoichiometric zirconia phase was quit unlikely. These phenomena have not normally associated to thermal diffusivity, but might increase it by shortening the intrinsic mean free path of phonons in zirconia.
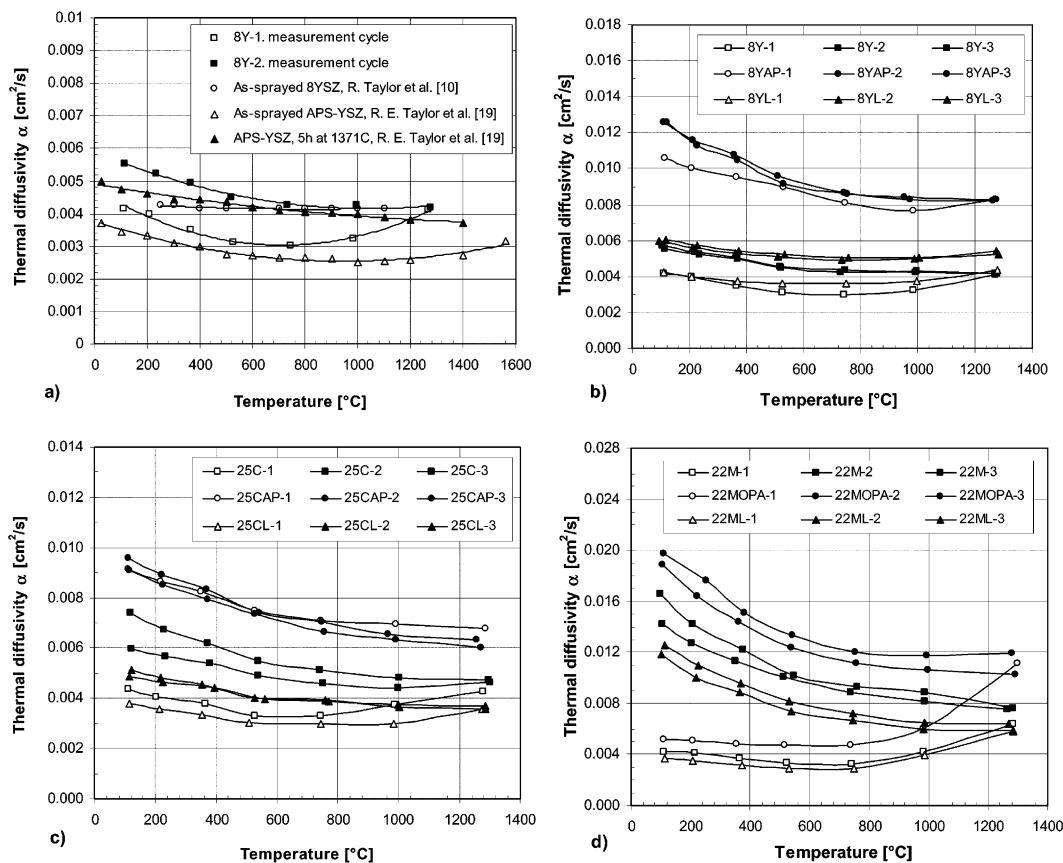
Fig. 4. Thermal diffusivity $\alpha(T)$ results of the (a) 8Y coatings compared to the reference data, (b) 8Y based coatings, (c) 25C based coatings and (d) 22M based coatings.

For all coatings the thermal diffusivity difference of the first two successive runs was quite high at low temperatures, but almost negligible at maximum temperature of 1300 °C. This can be explained by two different heat transfer mechanisms that dominate at different temperatures. At low temperatures the heat transfer in plasma sprayed zirconia is mainly based on phonon conductivity which is affected strongly by the microstructural features of coating like porosity and microcracks. At high temperatures above 1200 °C, in addition to phonon conductivity, the photon (radiation) conductivity takes place. As photon conductivity is not so much influenced by the microstructural features the results were equalized at temperatures close to 1250 °C.

Thermal diffusivity of the 8YL coatings was little higher if compared to the as-sprayed coatings. Even if it was impossible to determine the thermal diffusivity of the laser-glazed zone itself, it likely was higher than the normal structure of the as-sprayed coating because of the very low porosity and vertically oriented columnar grains. Aluminium phosphate sealing increased significantly thermal diffusivity of the 8Y coating. This is due to the sealant penetration into the coating interlamellar cracks and pores and related porosity decrease. Thermal diffusivity of the 8YAP in the second and third

runs could also be affected increasingly by the presence of the m–ZrO_2.

Thermal diffusivity of the ceria stabilized zirconia coatings was rather close to that of the yttria stabilized zirconia, see Fig. 4c. In as-sprayed 25C coating the $\alpha(T)$ was increased after the first run, but also in some degree after the second run. So the structural changes had taken place more steadily in 25C than in 8Y coating. The same behaviour was seen in thermal expansion study even though the differences were much smaller. Thermal diffusivity of the 25CL was lower than in the as-sprayed coatings. In the 25CL coating the segmentation cracks were non-vertically oriented, so they possibly have lowered thermal diffusivity. The $\alpha(T)$ of the 25CAP coatings did not varied much in successive measurement runs. Even if the thermal diffusivity of the aluminium phosphate sealed 25CAP coating was rather high, it was much lower than in the case of 8YAP coatings.

In all 22M based coatings significant increase of $\alpha(T)$ was observed in the first run at the temperature range of 800–1000 °C. This was mainly caused by the precipitation of the MgO from the zirconia matrix leading to unstabilization of the cubic/tetragonal zirconia (c/t–ZrO_2 m–ZrO_2). The crack structure in the laser-glazed 22ML coating was almost similar to 25CL coating and

so for that reason the α(T) of the 22ML was lower if compared to as-sprayed 22M coatings. Although some sintering based structural changes in the 22M based coatings might had occurred, the high thermal diffusivity values at low temperature were mainly caused by the presence of the MgO and m–ZrO$_2$.

3.4. Specific heat $C_P(T)$

Specific heat $C_P(T)$ of the as-sprayed coatings as a function of temperature is presented in Fig. 5 a and b. Measurements were carried out with free-standing coating specimens in argon atmosphere using platinum crucibles. The $C_P(T)$ curves were calculated as a mean value of three successive measurement cycles in order to lower the statistical errors. By using the reference sapphire sample the accuracy of the measurements were set within 4%. The trend of the $C_P(T)$ of the all three materials was rather similar and was increasing as a function of temperature. However, $C_P(T)$ of the 25C coating was little lower than that of 8Y coating. Respectively $C_P(T)$ of the 22M coating was higher in some degree than that of 8Y coating. The differences of the $C_P(T)$ values of these three materials were probably based on their chemical compositions. Besides, in the 25C coating there was some free CeO$_2$ (cerianite) and respectively in 22M coating some free MgO (periclase). The $C_P(T)$ values, found from the literature,[30] for the pure CeO$_2$ were 0.370 J/g°C at 27 °C and 0.520 at 927 °C. So these values are lower if compared to corresponding values for 8Y coating, taken from the Fig. 5b. (0.420–0.470 J/g°C at 27 °C and 0.615–0.640 J/g°C at 927 °C). For pure MgO the $C_P(T)$ was found to be approximately 0.910 J/g°C at 1 °C and 1.350 J/g°C at 1073 °C,[31] which is much higher if compared to 8Y coating.

At the beginning of the study the specific heat measurements were performed using alumina crucible, but with that setup some systematic error occurred at high temperatures (> 600 °C). The origin of the systematic error was not clear and for that reason it was decided to

use only platinum crucible. However, the measurements, made by alumina crucible showed that the specific heat of the laser-glazed coatings was equal of the as-sprayed coatings. Even the different phase structure of some coatings, like the presence of the Mg$_2$Zr$_5$O$_{12}$ in 22ML coating, did not affect seemingly on the $C_P(T)$ results. Anyway, the amount of this phase in the entire specimen was really low, because the laser-glazed layer was relatively thin (50–100 μm). In the case of the phosphate sealed coatings some divergence, if compared to the as-sprayed coatings, were found in the first $C_P(T)$ measurement cycle, see Fig. 6. These measurements were performed also with the alumina crucible. The divergence in the first cycle $C_P(T)$ might be caused by the irreversible reactions of the sealant such as dehydration or crystallisation of the amorphous sealant. This was supported by the fact, that the deviation in $C_P(T)$ curve was not present in the second measurement cycle and that the results were close to the as-sprayed coatings. In any case the accurate interpretation of the specific heat data at high temperature, based on the measurements done with alumina crucible, was difficult. For that reason, and because of the limited time schedule, it was decided to use the $C_P(T)$ data of the as-sprayed coatings in thermal conductivity calculations for laser-glazed and phosphate sealed coatings.

A lot of effort was put on determining the $C_P(T)$ in different conditions in order to find the most reliable way to perform the measurements. The specimens were prepared as free-standing coatings and powderized specimens and the measurements were performed in air and in argon atmospheres. Experience was also gathered using crucible materials Al$_2$O$_3$ and platinum. In any case it was found that the most reliable measurements were obtained with free-standing coating specimens in argon atmosphere using platinum crucible.

3.5. Thermal conductivity $k(T)$

Thermal conductivity results were calculated using the equation $k(T) = α(T)*C_P(T)*ρ_B$, where $α(T)$ is thermal
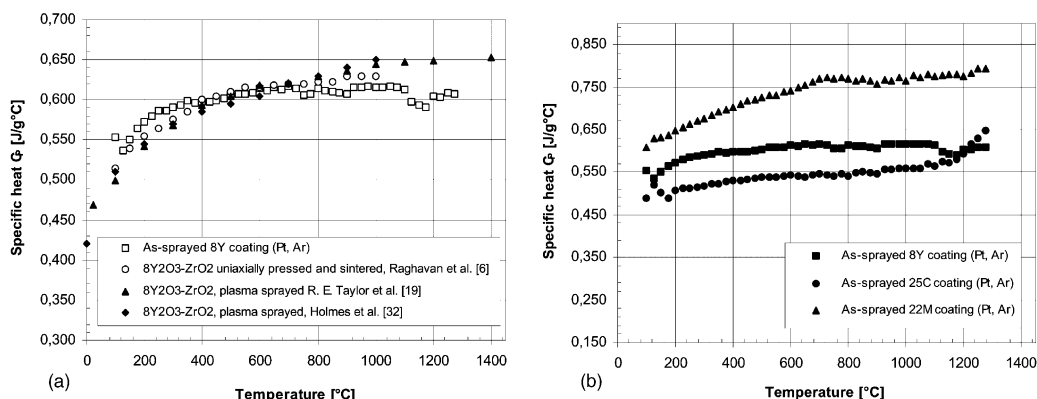

Fig. 5. Specific heat $C_P(T)$ results (a) as-sprayed 8Y coating compared to the reference data[6,19,32] and (b) all as-sprayed coatings.

diffusivity, $C_P(T)$ specific heat and ρ_B bulk density of the coating. Specific heat $C_P(T)$ data of the as-sprayed coatings were used in the calculations also for the modified coatings, as described in previous chapter. The results of two successive measurement cycles are presented in Fig. 7 a–d. The data found from the literature[6,15] for $8Y_2O_3$–ZrO_2 was compared to the results of 8Y coating, see Fig. 7a. Results are well in line with the
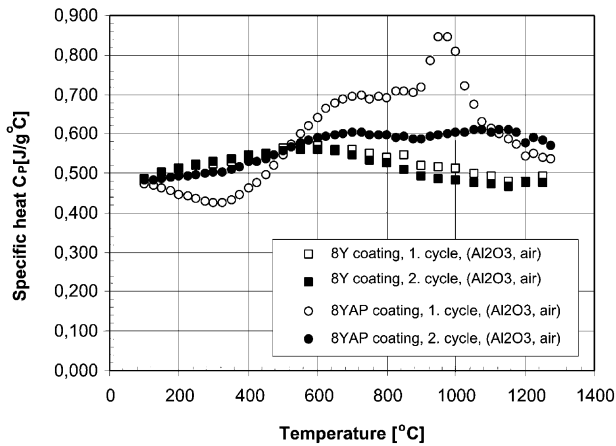
data of plasma sprayed $8Y_2O_3$–ZrO_2, determined by Dutton et al.[15] In Fig. 7a it can be seen that thermal conductivity of bulk yttria stabilized zirconia is about two-fold compared to plasma sprayed zirconia. In Fig. 7a it is also demonstrated high $k(T)$ values of pure m–ZrO_2, especially at low temperatures.

As the calculated thermal conductivities include all the results ($\alpha(T)$, $C_P(T)$, ρ_B) presented previously in this paper, the effect of the same structural changes on heat transfer can also be seen here. In all coatings $k(T)$ was obviously higher in the second measurement cycle. In 8Y and 25C based coatings this was mainly due to the better integrity of the lamellar structure induced by the sintering based phenomena. Zhu and Miller [11] demonstrated by isothermal $k(T)$ measurements at 990, 1100 and 1320 °C that the major increase in $k(T)$ takes place during the first 5–10 h, depending on the temperature. It is also showed here that the major increase of the $k(T)$ occurs really fast, even during one measurement cycle (RT→1300 °C→RT). In 22M based coatings the increase of $k(T)$ was based on another mechanism. It was mainly caused by the precipitation of MgO, leading to unstabilization of c/t–ZrO_2 zirconia and formation of m–ZrO_2.

The modification processes had quite clear effects on thermal conductivity of TTBCs. The effect of laser-

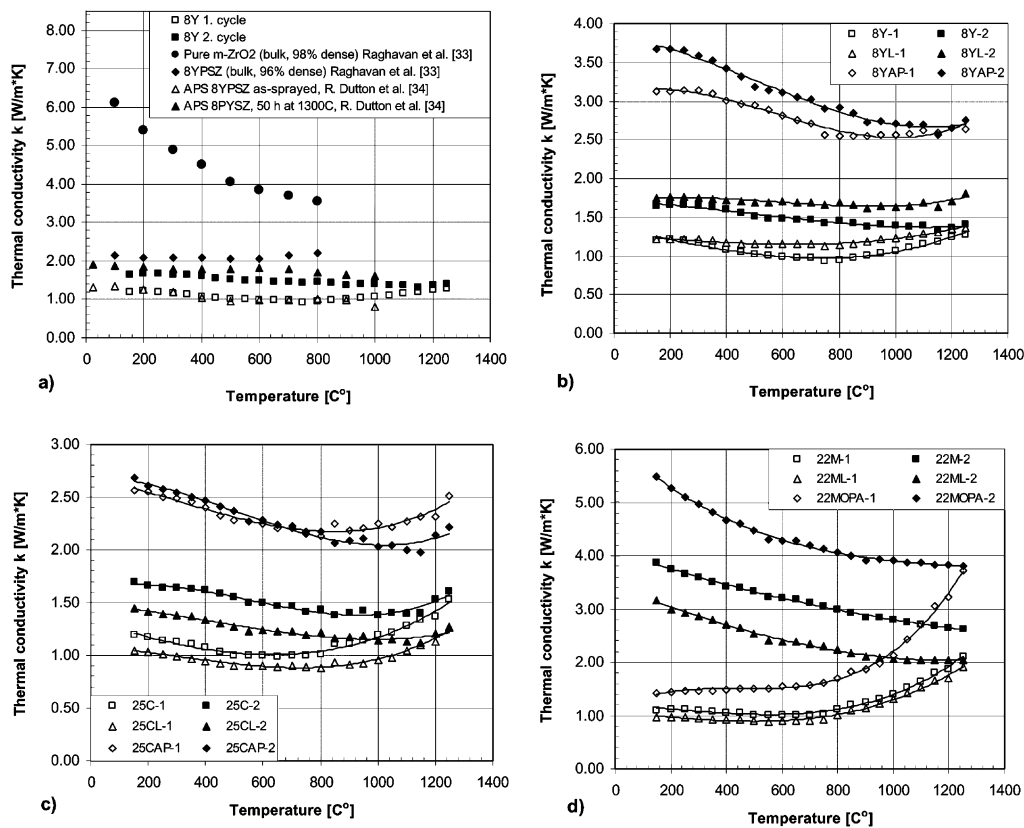Fig. 6. Specific heat $C_P(T)$ results of the 8Y and 8YAP coatings performed with alumina crucible in air.

Fig. 7. Thermal conductivity $k(T)$ results of the (a) 8Y coatings compared to the reference data, (b) 8Y based coatings, (c) 25C based coatings and (d) 22M based coatings.

glazing varied little between each coating material. In the 8YL coating, in which the segmentation cracks were straight in vertical direction, laser-glazing increased $k(T)$ slightly. But in the case of 25CL and 22ML coatings the effect was opposite. This can be explained by the fact that the segmentation cracks in 25CL and 22ML coatings were not perfectly vertically oriented and even some lateral branching cracks were found in optical microscopy studies below the laser-glazed layer. In the phosphate sealed coatings the sealant filled the cracks and pores and significantly increased $k(T)$. In the case of 8YAP and 22MOPA coatings, the sealant induced or accelerated unstabilization of zirconia structure which further increased thermal conductivity values.

4. Summary

In this paper the thermal properties of the modified TTBCs were determined and discussed. Coating microstructures were characterized in addition to thermal expansion, thermal diffusivity, specific heat and thermal conductivity. The main results can be summarized as follows:

- It was shown that the high temperature exposure up to 1300 °C increased the thermal conductivity of all TTBCs. In 8Y and 25C based coatings this was mainly caused by the sintering based phenomena in which the lamellae contact was improved at splat boundaries. In 22M based coatings thermal conductivity was increased significantly by precipitation of MgO, which led to unstabilization of c/t–ZrO_2 zirconia and formation of m–ZrO_2.
- Laser glazing had only slight effect on thermal conductivity of TTBCs. Thermal conductivity was increased in some degree if the segmentation cracks were oriented vertically like in the case of 8YL coating. But if the orientation of the segmentation cracks differed from the vertical direction or if the cracks were branched, thermal conductivity was decreased. This was observed in the case of 25CL and 22ML coatings.
- Phosphate based sealing treatments increased significantly thermal conductivity of TTBCs by reducing the porosity and filling the cracks and interlamellar spacings. High temperature stability of the TTBCs was also decreased by phosphate sealing.

Acknowledgements

References

1. Klemens, P. G. and Gell, M., Thermal conductivity of thermal barrier coatings. *Materials Science and Engineering*, 1998, **A245**, 143–149.
2. Klemens, P. G., Phonon scattering by oxygen vacancies in ceramics. *Physica B*, 1999, **263-264**, 102–104.
3. Nicholls, J. R., Lawson, K. J., Johnstone, A. and Rickerby, D. S., Methods to reduce the thermal conductivity of EB-PVD TBS's. *Surf. Coat. Technol.*, 2002, **151–152**, 383–391.
4. An, K., Ravichandran, K. S., Dutton, R. E. and Semiatin, S. L., Microstructure, texture and thermal conductivity of single-layer and multilayer thermal barrier coatings of Y_2O_3-stabilized ZrO_2 and Al_2O_3 made by physical vapor deposition. *J. Am. Ceram. Soc.*, 1999, **82**(2), 399–406.
5. Ravichandran, K. S., An, K., Dutton, R. E. and Semiatin, S. L., Thermal conductivity of plasma-sprayed monolothic and multi-layer coatings of alumina and yttria-stabilized zirconia. *J. Am. Ceram. Soc.*, 1999, **82**(3), 673–682.
6. Raghavan, S., Wang, H., Dinwiddie, R. B., Porter, W. D. and Mayo, M. J., The effect of grain size, porosity and yttria content on the thermal conductivity of nanocrystalline zirconia. *Scripta Materialia*, 1998, **39**(8), 1119–1125.
7. Raghavan, S., Wang, H., Porter, W. D., Dinwiddie, R. B. and Mayo, M. J., Thermal properties of zirconia Co-doped with tri-valent and pentavalent oxides. *Acta Materiali*, 2001, **49**, 169–179.
8. Rudajevova, A., Thermal diffusivity of plasma-sprayed coatings of ZrO_2 with 8 wt.% Y_2O_3 and ZrO2 with 25 wt.% CeO_2. *Thin Solid Films*, 1993, **223**, 248–252.
9. Sodeoka, S., Suzuki, M., Ueno, K., Sakuramoto, H., Shibata, T. and Ando, M., Thermal and mechanical properties of ZrO_2–CeO_2 plasma-sprayed coatings. *J. Therm. Spray Techn.*, 1997, **6**(3), 361–367.
10. Taylor, R., Brandon, J. R. and Morrel, P., Microstructure, composition and property relationship of plasma sprayed thermal barrier coatings. *Surf. Coat. Technol.*, 1992, **50**, 141–149.
11. Zhu, D. and Miller, R. A., Thermal conductivity and elastic modulus evolution of thermal barrier coatings under high heat flux conditions. *J. Therm. Spray Techn*, 2000, **9**(2), 175–180.
12. Zhu, D., Miller, R. A., Nagaraj, B. A. and Bruce, R. W., Thermal conductivity of EB-PVD thermal barrier coatings evaluated by a steady-state laser heat flux technique. *Surf. Coat. Technol.*, 2001, **138**, 1–8.
13. Zhu, D. and Miller, R. A., Sintering and creep behavior of plasma-sprayed zirconia- and hafnia-based thermal barrier coatings. *Surf. Coat. Technol.*, , 1998, **108–109**, 114–120.
14. Steffens, H. D., Babiak, Z. and Brandl, W., Thermal barrier coatings: some aspects of properties design. In *Thermal Spray Coatings: Properties, Processes and Applications: Proceedings of the Fourth National Thermal Spray Conference 1991*, ed. Thomas F. Bernecki. ASM International, Materials Park, OH-USA, 1992, pp. 289–294.

15. Dutton, R., Wheeler, R., Ravichandran, K. S. and An, K., Effect of heat treatment on the thermal conductivity of plasma-sprayed thermal barrier coatings. *J. Therm. Spray Techn.*, 2000, **9**(2), 204–209.

16. Vaβen, R., Czech, N., Mallener, W., Stamm, W. and Stovera, D., Influence of impurity content and porosity of plasma-sprayed yttria-stabilized zirconia layers on the sintering behaviour. *Surf. Coat. Technol.*, 2001, **141**, 135–140.

17. Wang, H. and Dinwiddie, R. B., Characterization of thermal barrier coatings using thermal methods. *Advanced Engineering Materials*, 2001, **3**(7), 465–468.

18. Schichting, K. W., Padture, N .P. and Klemens, P. G., Thermal conductivity of dense and porous yttria-stabilized zirconia. *Journal of Materials Science*, 2001, **36**, 3003–3010.

19. Taylor, R. E., Wang, X. and Xu, X., Thermophysical properties of thermal barrier coatings. *Surf. Coat. Technol., 120-*, 1999, **121**, 89–95.

20. Wang, H. and Dinwiddie, R. B., Reliability of laser flash thermal diffusivity measurements of the thermal barrier coatings. *J. Therm. Spray Techn.*, 2002, **9**(2), 210–214.

21. Cernuschi, F., Bianchi, P., Leoni, M. and Scardi, P., Thermal diffusivity/microstructure relationship in Y-PSZ thermal barrier coatings. *J. Therm. Spray Techn.*, 1999, **8**(1), 103–109.

22. Slifka, A. J., Filla, B. J., Phelps, J. M., Bancke, G. and Berndt, C. C., Thermal conductivity of a zirconia thermal barrier coating. *J. Therm. Spray Techn.*, 1998, **7**(1), 43–46.

23. Segostianov, I. and Kachanov, M., Anisotropic thermal conductivities of plasma-sprayed thermal barrier coatings in relation to the microstructure. *J. Therm. Spray Techn.*, 2002, **9**(4), 478–482.

24. Nesbitt, J. A., Thermal modelling of various thermal barrier coatings in a high heat flux rocker engine. *Surf. Coat. Technol.*, 2000, **130**, 141–151.

25. Ahmaniemi, S., Vippola, M., Vuoristo, P., Mäntylä, T., Cernuschi, F., and Lutterotti, L., Modified thick thermal barrier coatings, Part I: microstructural characterization. *Journal of European Ceramic Society* (in press).

26. Ahmaniemi, S., Vuoristo, P. and Mäntylä, T., Sealing procedures for thick thermal barrier coatings. *J. Therm. Spray Techn.*, 2002, **11**(3), 320–332.

27. Ahmaniemi, S., Tuominen, J., Vuoristo, P. and Mäntylä, T., Improved sealing treatments for thick thermal barrier coatings. *Surf. Coat. Technol., *, 2002, **151–152**, 412–417.

28. Young, R. A., *The Rietveld Method*. Oxford University Press, Walton Street, Oxford, UK, 1993.

29. Scardi, P., Lutterotti, L. and Galvanetto, E., *Surf. Coat. Technol.*, 1993, **61**, 52–59.

30. Lackey, W. J., Stinton, D. P., Cerny, G. A., Fehrenbacher, L. L. and Schaffhauser, A. C., Ceramic coatings for heat engine materials status and future needs. *ORNL/TM-8959*, 1984.

31. Lynch, J. F., ed., *Engineering Property Data on Selected Ceramics Volume III, Single Oxides, MCIC-HB-07 Report/July 1981*. Metals and Ceramics Information Center, Batelle, Columbus Laboratories, Columbus, Ohio, USA, 1981.

32. Holmes, R. R. and McKechnie, T. N., Vacuum application of thermal barrier plasma coatings. In *NASA Marshall Space Flight Center Advanced Earth-To-Orbit Propulsion Technology vol 1*, eds. Richmond, R.J., Wu, S.T., 1988, pp. 692–702.